ELM Pacing with High Frequency Multi-species Impurity Granule Injection in NSTX-U H-Mode Discharges

R. Lunsford, A. Bortolon, A.L. Roquemore, D.K. Mansfield, M.A. Jaworski, R. Kaita, R. Maingi, A. Nagy and the NSTX-U team
Email: rlunsfor@pppl.gov
Princeton Plasma Physics Laboratory, PO Box 451, Princeton, NJ 08543 USA

Abstract

Employing a neutral gas shielding model, benchmarked with lithium granule ablation experiments performed on DIII-D, the pedestal atomic deposition characteristics for three different species of granule: lithium, boron, and carbon; have been modelled for NSTX-U discharges. Simulations of 300, 500 and 700 micron diameter granules injected at 50 m/sec are presented for NSTX-U L-mode type plasmas as well as H-mode discharges with low natural ELM frequencies. Additionally, ablation calculations of 500 micron granules of each species are presented at velocities ranging from 50 – 150 m/sec. These simulations estimate the ablation rate and mass deposition location with respect to the plasma density profile. In H-mode type discharges these simulations show that the majority of the injected granule is ablated within or just past the steep gradient region of the discharge. At this radial position, the perturbation to the background plasma generated by the ablating granule can lead to conditions advantageous for the rapid triggering of an ELM crash event.

1. Introduction

The ability to control Edge Localized Modes(ELMs) is required for successful operation of next generation plasma devices such as ITER. For discharges with a naturally low ELM frequency, on the order of a few Hertz, the impurity ejection provided by the spontaneously occurring ELMs is projected to be insufficient to control the buildup of impurities within the plasma core. To maintain a low Z_{eff}, the period between the ELMs must be smaller than the edge to core transport times of the sputtered divertor and first wall material. During the hydrogen/helium operational phase of ITER, the intrinsic ELM frequency is anticipated to be too low to provide sufficient impurity exhaust, and must be augmented through one or more techniques[1, 2]. As the plasma current is increased, the spatial footprint of the energy exhausted to the plasma facing components by ELMs narrows and the unmitigated peak heat flux can exceed material integrity limits. Previous experiments[3] have demonstrated that, in certain circumstances, there is an inverse relationship between the frequency of the triggered ELM and the peak heat flux contained within the mode. Thus to generate the required mitigation, a rapid triggering of ELMs is employed to reduce the peak heat flux. While recent results have called into question the efficacy of pacing in metal walled tokamaks[4, 5], ELM pacing is one of a few baseline ELM heat flux mitigation strategies for ITER.

The injection of deuterium pellets into the edge of a magnetically confined plasma is one of the methods used to generate on-demand triggering of ELMs through the seeding of a torodially localized pressure perturbation[6, 7]. These stimulated ELMs display an inverse relationship between the pellet injection frequency and the resultant peak heat flux, thus reducing the efflux of particles and energy to a level tractable for the plasma facing

components. At DIII-D the injection of sub-millimeter lithium granules to trigger and pace ELMs has been shown to produce a similar heat flux mitigation effect[8] under certain conditions.

The granule injector apparatus first employed at EAST[9], and then on DIII-D and installed on NSTX-U utilizes a dual-bladed rotating PEEK impeller driven at rotation frequencies of up to 250 Hz, allowing for pacing frequencies of up to 500 Hz and injection velocities of up to 150 m/sec. This impeller redirects gravitationally accelerated solid impurity microgranules horizontally into the low field side of the discharge. The ablation of the granules generates an overdense flux tube which drives an MHD ballooning-type instability resulting in a triggered ELM. Utilizing the lithium granule injection experiments at DIII-D to calibrate a neutral gas shielding (NGS) model[10] for granule ablation and mass deposition we estimate the fractional portion of the granule mass deposited at the top of the pedestal. It is believed that this metric is directly correlated to the probability that the injected granule will trigger an ELM. This model, applied to NSTX-U H-Mode discharges, for a granule injector operating at a midrange injection velocity of 100 m/sec, projects that an ablating granule will deliver nominal central mass deposition distances of approximately 3 cm and 8 cm for 500 micron lithium and carbon granules respectively. Reducing the impeller frequency ameliorates the impurity influx to the discharge core by an outward shift in the depositional barycenter allowing the injected mass to remain closer to the separatrix where up to 80% of the granule material is promptly flushed by the stimulated ELM[11] .

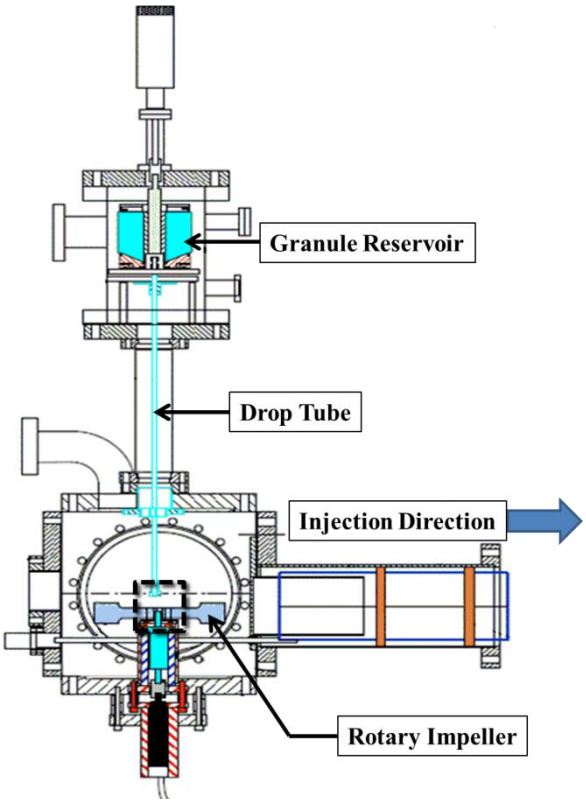

Figure 1: Granule Injector Cutaway. Granules travel from the reservoir, down the drop tube and are driven into the discharge by the impeller. The dashed black box denotes the region of interest for the photograph series in Figure 2

The remainder of this paper discusses the granule injector apparatus, details the granule ablation and mass deposition analysis model and then utilizing the experiments at DIII-D as a benchmark extrapolates the results of these injection characteristics in NSTX-U discharges.

2. Impurity Granule Injector Apparatus

The impurity granule injector (IGI) was designed at PPPL and first utilized during lithium granule injection experiments on the EAST tokomak. As is shown in Figure 1, the granules are housed in a reservoir positioned above the injection chamber. A vibrating piezoelectric disk at the bottom of the reservoir is driven at a resonance of 2250 Hz. This frequency generates a node at the center of the disk driving the granules toward a circular aperture located above the drop tube. Granules fall into the drop tube where they are gravitationally accelerated. At the end of the tube a rapidly rotating dual bladed turbine impeller redirects

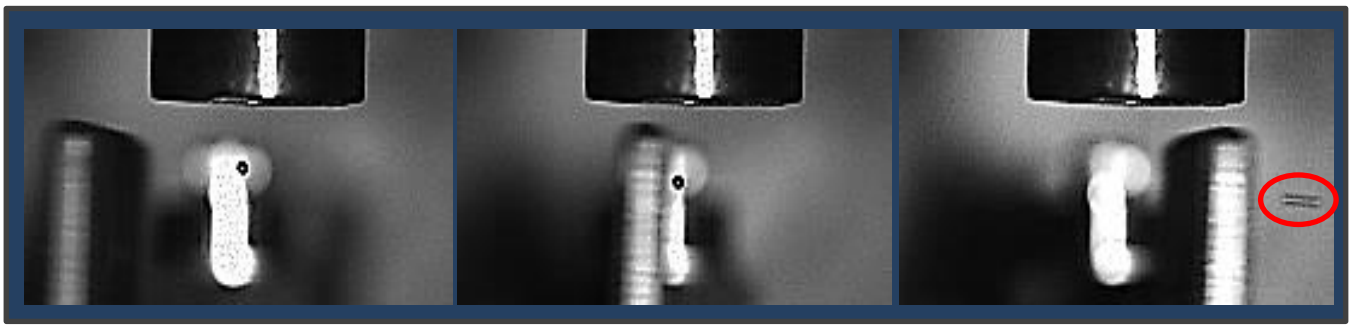

Figure 2 : Horizontal injection of a 700 micron carbon microsphere. Exposure time is 50 microseconds and interframe time is 200 microseconds. Motion blur of the rightmost granule (circled) gives an estimated velocity of 45 m/sec.

the granules into the edge of the discharge as shown in Figure 2. By adjusting the voltage used to drive the piezoelectric disk the granule drop frequency can be roughly controlled. Likewise, by altering the rotation speed of the impeller, the granule injection speed and maximum injection frequency can be adjusted. Granule drop frequencies can be varied from a single granule injection up to approximately 300 Hz. Injection velocities can range from 40 - 100 m/sec for malleable granules such a lithium, and from 40 - 150 m/sec for inelastic granules such as vitreous carbon. This variation is due to inelastic granule deformation observed during paddle impact. Velocities below 40 m/sec are impractical due to gravitational parabolic decay of the granule during horizontal injections. The dropper and impeller method of granule delivery provides a simple and robust method of injection at a range of frequencies, granule sizes (100 - 1000 micron diameters) and velocities. Note however that the dropper disk and the impeller are uncoupled, leading to an asynchronous delivery of granules. Further details about the system can be found in Refs [5, 12, 13].

3. Neutral Gas Shielding(NGS) model of granule ablation

Upon injection of a granules into the low field side of a fusion research plasma, electron heat conduction along the magnetic field lines causes the outer layer of the granule to rapidly ablate. As shown in Figure 3, the ablatant forms a dense neutral cloud partially shielding the granule from the surrounding plasma. Further heat input results in an ionization of the ablatant material that is conducted away from the granule along field lines at ion acoustic speed. This quasi-stasis of granule and neutral cloud is maintained until the granule can no longer replace the ablatant material lost to ionization. Observations of injected granules confirm the overall cigar shape of the ablation cloud [14] and the occultation of the injected granule during injection is indicative of the described dense neutral cloud. The mass deposition of these granules into the edge of the discharge

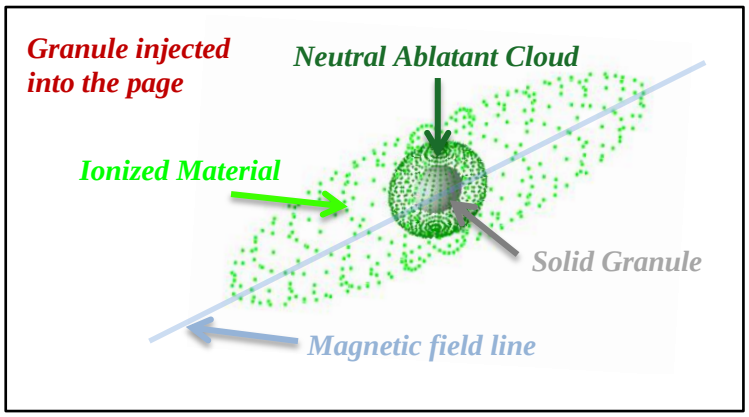

Figure 3: Ablation characteristics of an injected solid granule.

leads to a peaking of the localized plasma pressure, and the creation of an overdense flux tube which becomes 3-D ballooning unstable, resulting in an ELM.

Following Refs [15, 16] the ablation rate (G) of the injected granule is given by Equation (1)

$$G = 4\pi q_s \eta \xi_g f_B \tag{1}$$

where f_B is the combined field directed anisotropy and flux screening parameter, and is numerically equal to 0.08 [10]; $\boldsymbol{q_s}$ is the heat flux variable as described by equation (2)

$$q_s = \frac{1}{2}\, n_e T_e \left(\frac{8T_e}{\pi m_e}\right)^{1/2} \tag{2}$$

with the nominal definitions of the plasma parameters $\boldsymbol{n_e}$, $\boldsymbol{T_e}$, and $\boldsymbol{m_e}$. The characteristic granule parameter ($\boldsymbol{\xi_g}$) is given by equation (3)

$$\xi_g = \frac{{r_g}^2}{n_g} \left[\Delta H + \frac{10}{3} T_S\right]^{-1} \tag{3}$$

and is comprised of the granule radius ($\boldsymbol{r_g}$), the solid granule density ($\boldsymbol{n_g}$), the sublimation energy of the granule ($\boldsymbol{\Delta H}$) and the surface temperature of the ablating granule ($\boldsymbol{T_s}$) which for these calculations is assumed to be either the boiling point, or vaporization temperature of the granule material in question. The density, sublimation energy, and surface temperature of the candidate granule materials as well as the estimated number of electrons per injected granule are summarized in Table 1. Finally the cloud shielding parameter ($\boldsymbol{\eta}$) represents the fractional efficiency of the neutral ablated material in shielding the solid granule from the incoming electron flux and is experimentally determined as described in the following section

	Density (atoms/m^3)	Sublimation Energy (eV)	Granule Surface Temperature (eV)	Number of electrons / 500 micron granule
Lithium	4.6×10^{28}	1.6	0.14	9.1×10^{18}
Boron	1.3×10^{29}	5.3	0.36	5.2×10^{19}
Carbon	1.12×10^{29}	7.5	0.34	4.2×10^{19}

Table 1: Granule Composition Factors

4. Numerical Simulation of Granule Injections into NSTX-U discharges

A calibration of the neutral gas shielding model described in the previous section was performed during lithium granule injection experiments on DIII-D[17]. A high speed camera located at the back of the IGI system and optically aligned radially inward along the injection vector was used to observe the ionization emission from the injected granules. By fitting the time envelope of the ablation event to the calculation of the granule lifetime, the cloud shielding parameter $\boldsymbol{\eta}$ is experimentally determined. It is then be utilized to ascertain a decay rate for the injected granule radius thus resulting in a mass deposition rate within the plasma and consequently a penetration depth of the solid granule. Utilizing this technique we

found the neutral gas shielding model to be effective at recreating the emission profile observed in the experiment.

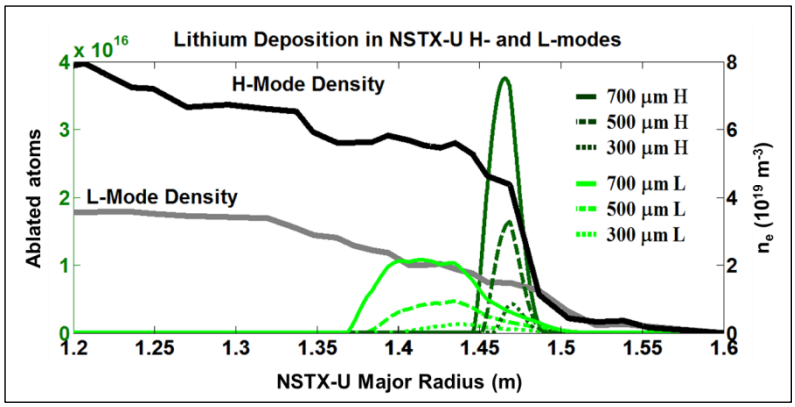

Figure 4 : Simulated ablatant deposition location for 500 micron lithium granules injected at 50 m/sec into NSTX-U H and L-modes.

4.1 Variations in granule size and plasma parameters

The experimentally obtained value for the cloud shielding parameter was adopted for the simulation of granule injection into NSTX-U discharges to project the pedestal atomic deposition characteristics for three different species of granules (Li, B, C). Simulated granule diameters of 300, 500, and 700 microns are injected at 50 m/sec into both an NSTX-U L-mode (204563) as well as an NSTX-U H-mode (204118) with low natural ELM frequency. Temperature and density for the L-mode were sampled at 650 msec, plasma parameters at this time were: B_T = 0.63 T, I_P = 640 kA, W_{Tot} = 65 kJ, $\beta_N \approx 1.8$, and $q_{95} \approx 4.8$. The H-mode profile was also sampled at 650 msec and the resultant plasma parameters were: B_T = 0.63 T, I_P = 1 MA, W_{Tot} = 334 kJ, $\beta_N \approx$ 4.5, and $q_{95} \approx 6.7$. The granule sizes stated above were chosen during the design phase of the granule injector apparatus as spanning the space most likely to trigger ELMs while generating a minimal impurity overburden to the receiving plasma. The simulation velocity represents a minimal effective injection velocity of the granule injector. It was chosen to ensure granule penetration of the discharge while resulting in the most outboard deposition of the ablated material and thus mitigate the core contamination.

In Figure 4, the calculated depositional profiles of injected lithium granules into the edge of NSTX-U discharges are shown. The darker traces are representative of granules injected into an H-mode type discharge, while the lighter traces are calculations of the ablatant deposition into an L-mode discharge. As is shown, the mass deposition is strongly peaked with the granule injections into H-mode and the penetration depth of the injected granules is commensurately reduced by almost a factor of 3 when compared to injections in L-mode discharges. The strong peaking is coincident with the H-mode pedestal, as measured by Thompson scattering and shown by the black trace displayed on the figures. This co-location of the ablatant deposition and the steep gradient region results in a localized pressure perturbation which is beneficial for the triggering of an edge localized mode.

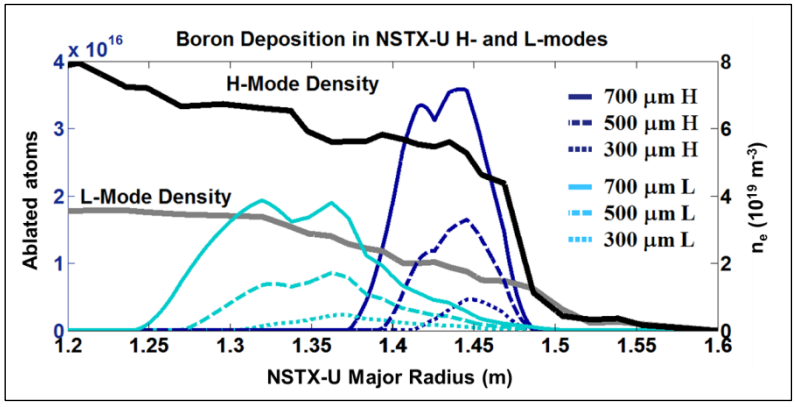

Figure 5 : Simulated ablatant deposition location for 500 micron boron granules injected at 50 m/sec into NSTX-U H and L-modes.

Figure 5 displays the mass deposition location for boron granules. While experiments will be undertaken with boron carbide granules, the simulations were performed with pure boron granules for ease of modelling. The higher sublimation energy of boron granules results in a deeper penetration than those seen with lithium, while the higher density results in a respectively larger number of atoms introduced into the edge discharge for an injected granule of the same size. This results in a greater density perturbation than seen with lithium. The simulation of carbon granule injection shown in figure 6 displays a similar behavior. However, despite a similar density to boron, the larger sublimation energy of the carbon granule (7.5 eV vs. 5.3 eV) results in an even deeper penetration and consequently a mass distribution that is not as strongly peaked. For the largest granule injections into L-mode type plasmas even at this low injection velocity the granule does not fully ablate until it has reached ~30 cm into the discharge.

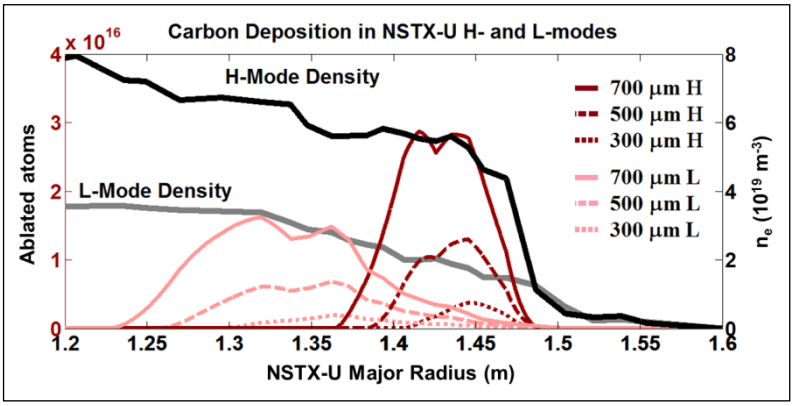

Figure 6 : Simulated ablatant deposition location for 500 micron carbon granules injected at 50 m/sec into NSTX-U H and L-modes.

4.2 Variations in granule velocity

To further explore the mass deposition characteristics of injected impurity granules we now focus primarily on the midsize (500 micron) granules and vary the injection velocity over the range available to the granule injector (40 – 150 m/sec). Altering the injection velocity of the granule, presented in the lower three intensity graphs in Figure 7, can further modify the mass deposition location, allowing tuning of the localized pressure perturbation and thus effecting the ELM triggering efficiency. By reducing the rotation speed of the impeller, the peak mass deposition location is translated closer to the top of the pedestal. At this location the pressure profile generated by the granule can be added to the preexisting pedestal pressure gradient, leading to a set of characteristics advantageous for ELM triggering while affecting a minimal perturbation to the core plasma. As shown in the upper panel of Figure 7, variations in the depositional barycenter can range from approximately 3 cm for lithium to 8 cm for the same size (500 microns) and velocity (100 m/sec) carbon granule.

Lithium granules, with their relatively low sublimation energy are found to ablate rapidly at the edge of the discharge independent of the injection velocity. In contrast the velocity depositional tuning effect can substantially vary the ablation profile in the boron and carbon granules. This insensitivity to velocity could explain the findings of previous experiments[5] which reported ELM triggering efficiency to be primarily dependent upon the size of the granule with the injection velocity presenting minimal effect.

This calculation of the mass deposition location is predicated on the granule maintaining a constant velocity during injection. There exists the possibility of a non-uniform granule ablation, as observed in deuterium pellet injection whereby there is an increased ablation rate on the high filed side of the granule due to the elevated heat flux. This increased ablation rate generates a so called “rocket effect”[18] which decelerates the granule. An extended imaging

suite to record full granule injections from multiple locations, as is planned for the NSTX-U granule injection experiments, should resolve this issue.

6. Conclusion

The injection of pellets or granules into the edge of a fusion research plasma has been shown to trigger ELMs through the seeding of a torodially localized pressure perturbation which drives a region of the discharge past the peeling/ballooning stability threshold. This on-demand ELM triggering allows for density control and is a ITER baseline mechanism for ELM mitigation through the utilization of pacing. Triggering these ELMs through the injection of low Z impurity granules has the added benefit of decoupling the pacing mechanism from the fueling cycle and ameliorating the pumping requirements from high speed pacing. That being said, impurity granule pacing does create issues of dust generation and a possible impurity overload of the discharge. To codify these issues, further study is required.

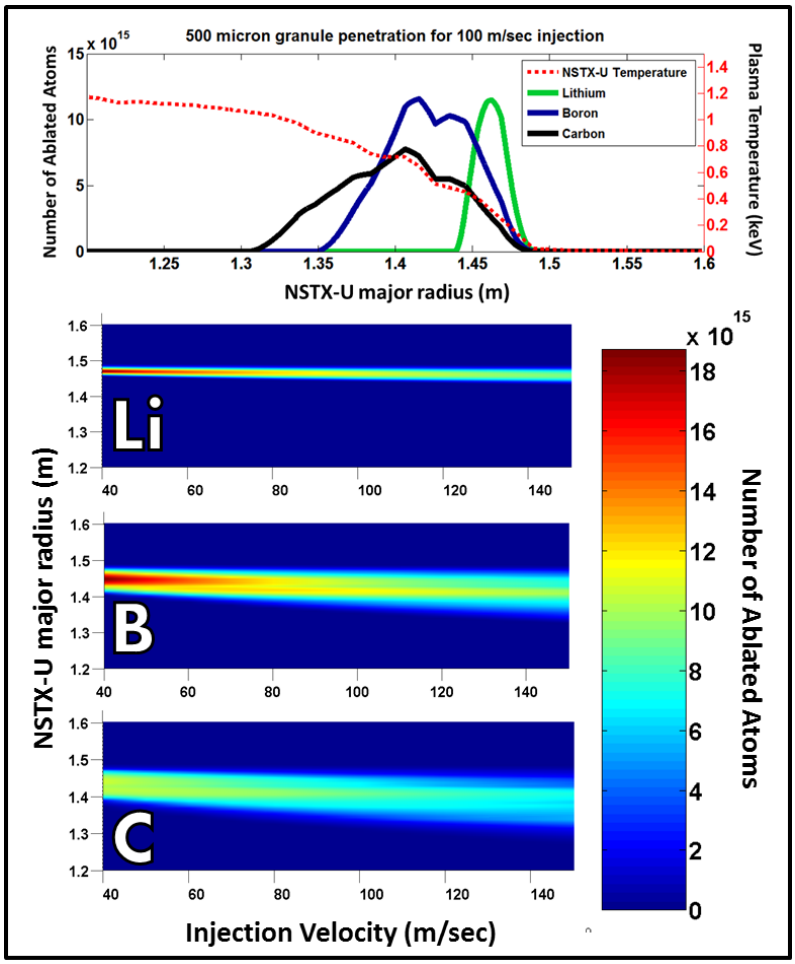

Figure 7: Mass deposition location for injected granules of differing species. The top panel displays the ablatant deposition for three 500 micron granules injected at 100 m/sec. The bottom three panels illustrate the variation in mass deposition location for alternate injection velocities. In these graphs the granule injection direction is from top to bottom.

We have utilized an NGS ablation model to characterize the injection of lithium, boron and carbon granules. The granule shielding parameter was experimentally determined by monitoring the ablation duration for several sizes of lithium granule during their injection into DIII-D H-Mode plasmas. Adopting this parameter we are able to project the ablation rates and mass deposition profiles for multi-species granule injections on NSTX-U. The NSTX-U discharges utilized for this simulation are taken from the first operational year of the upgraded system. Looking at the NGS model (eq 2) we estimate that these penetration depths will be reduced by a factor proportional to $q_s \sim n_e T_e^{3/2}$ as the full NSTX-U capabilities are realized. This includes increases in B_T from 0.65 T to 1.0 T, IP from 1 MA to 2 MA, and P_{NB} increased from 5 MJ to ~14 MJ.

As shown, by adjusting granule size, composition and velocity the edge pressure perturbation resultant from an injected granule can be tailored to the necessary requirements for ELM triggering while minimizing any deleterious effects upon discharge performance. Utilizing

lithium, boron and carbon granules in future injection experiments facilitates the extrapolation of plasma response to the injection of beryllium granules which is a native ITER first wall material. Extrapolation to this material then allows a benchmarking of the requirements for impurity granule pacing on next generation fusion devices such as ITER. The expansion of this model to a species specific granule shielding parameter will be the focus of future work.

This work supported by US Department of Energy Contract No. DE-AC02-09CH11466

[1] T.E. Evans, J. Nucl. Mater. 438 (2013) S11-S18
[2] A. Loarte et al., Nucl. Fusion 54 (2014) 033007
[3] L.R. Baylor et al., Phys Rev Lett. 110 (2013) 245001
[4] P.T. Lang, et al.," Nucl. Fusion 53 (2013) 073010
[5] P.T. Lang, et al., Nucl. Fusion 54 (2014) 083009
[6] S. Futatani et. al., Nucl. Fusion 54 (2014) 073008
[7] L Baylor et al., J Nucl Mater 463 (2015) 104-108
[8] A. Bortolon et al., Nucl. Fusion 56 (2016) 056008
[9] D. K. Mansfield et al., Nucl. Fusion 53 (2013) 113023
[10] P.B. Parks et al., Nucl. Fusion 34 No. 3 (1994) 417
[11] L Baylor et. al., J Nucl. Mater 266-269 (1999) 457-461
[12] A.L. Roquemore et al., Fusion Eng. and Design 86 (2011) 1355
[13] D. K. Mansfield et al., Fusion Eng. and Design 85 (2010) 890
[14] H. W. Müller, et al., Nucl. Fusion 42 (2002) 301
[15] P. Parks et al.," Nucl. Fusion 28 (1988) 477
[16] G. Kocsis et al., PPCF 41 (1999) 881-898
[17] R. Lunsford et. al., Fusion Eng & Design (2016) *in press*
[18] H. W. Müller, et al., Nucl. Fusion **42** (2002) 301